Journal of Proton Therapy
ISSN 2469-5491
www.protonjournal.org

Uncertainty in dose per monitor unit estimates for passively scattered proton therapy: The role of compensator and patient scatter in prostate cases

Wayne Newhauser[1,2,3,4,*], Annelise Giebeler[1,2,5], Ronald Zhu[1,2], Uwe Titt[1,2], Andrew Lee[1,6], Rui Zhang[1,2,3,4]

[1]*Department of Radiation Physics and Radiation Oncology, The University of Texas MD Anderson Cancer Center, Houston, Texas, USA*
[2]*The University of Texas Graduate School of Biomedical Sciences at Houston, Houston, Texas, USA*
[3]*Department of Physics and Astronomy, Louisiana State University, Medical Physics Program, Baton Rouge, Louisiana, USA*
[4]*Mary Bird Perkins Cancer Center, Baton Rouge, Louisiana, USA*
[5]*Scripps Proton Therapy Center, Summers Ridge Road, San Diego, California, USA*
[6]*Texas Center for Proton Therapy, Irving, Texas, USA*

Article history:
Submission: May 11, 2015
First Revision: June 17, 2015
Acceptance: June 24, 2015
Publication: August 22, 2015

Cite this article as:
Newhauser WD, Giebeler A, Zhu R, Titt U, Lee A, Zhang R. Uncertainty in dose per monitor unit estimates for passively scattered proton therapy: The role of compensator and patient scatter in prostate cases. *Jour Proton Ther* 2015; 1:116. DOI: 10.14319/jpt.11.6

**Corresponding author:*
Wayne Newhauser, PhD; Mary Bird Perkins Cancer Center and Louisiana State University, Baton Rouge, LA, 70803, USA.

Abstract

Standard methods for determining dose per monitor unit values in a patient do not yet exist for proton therapy. Indeed, some aspects of *D/MU* estimation remain poorly understood, such as the conversion of absorbed dose in a water phantom to absorbed dose in a patient. This study focused on the water-to-patient absorbed dose conversion factor, F_{CSPS}, which accounts for differences in scatter (from the range compensator and internal patient anatomy) between patient treatments and their corresponding calibration irradiation in a homogeneous water-box-phantom. We estimated F_{CSPS} for 32 prostate fields using a pencil beam dose algorithm in the treatment planning system (TPS). The mean F_{CSPS} value was 1.006; its standard deviation of the mean was ±0.001. The lower bound for uncertainty in F_{CSPS}, μF_{CSPS}, was estimated for a subset of fields through comparisons of TPS dose predictions with measurements and Monte Carlo (MC) simulations. Comparison of TPS predictions and measurements yielded μF_{CSPS} of 0.4% - 0.8%. Comparison of TPS predictions and MC simulations yielded μF_{CSPS} < 0.3%. For a prostate treatment, a comparison of F_{CSPS} values from TPS predictions with the historical value of 1.0 yielded μF_{CSPS} < 3% and a mean μF_{CSPS} of 0.6%. Regardless of estimation method, μF_{CSPS} was approximately 1%, suggesting that uncertainty in F_{CSPS} for proton treatments of prostate cancer is clinically acceptable.

Keywords: Dose Per Monitor Unit; Prostate Cancer; Proton Therapy; Uncertainty

Original Article

1. Introduction

Proton therapy is gradually becoming more available to the general patient population.[1, 2] Specifically, the number of proton treatment centers increased from 15 to 46 from 2000 to 2014.[3] An analysis of cancers treated with proton therapy revealed that the most commonly treated diseases were uveal melanoma (35%) and prostate cancer (26%).[4] Of these, treatments for prostate cancer are of particular interest because of its high incidence.[5] In addition, recent studies report that relative to conventional photon radiotherapy, proton therapy for localized prostate cancer permits reduced dose to critical structures[6-13] and successful dose escalation[7, 14, 15]. However, because proton therapy was previously limited to a few centers worldwide, there have been no large-scale randomized clinical trials of proton vs. photon radiotherapy for prostate cancer.[16, 17] Thus, there is a strong impetus to standardize the dosimetry of proton radiotherapy so that patient treatment and outcome data can be directly

compared. In this respect, advisory bodies have published proton dosimetry protocols for determining proton beam output, or absorbed dose per monitor unit (*D/MU*) values, in water under reference conditions (such as the American Association of Physicists in Medicine[18], European Clinical Heavy Particle Dosimetry Group (ECHED)[19,20], International Commission on Radiation Units and Measurements[1], and the International Atomic Energy Agency[21]. Still, in contrast to photon and electron therapy, to date, a protocol to harmonize methods for estimating absorbed dose from proton therapy in a patient is lacking.

Nonetheless, progress is being made toward a more complete understanding of the determination of absorbed dose in a patient receiving proton therapy.[22-31] Specifically, progress includes the creation of a geometrical framework and an initial estimate of 1.0 for a water-to-patient absorbed dose conversion factor[22] as well as validation of Monte Carlo (MC)-simulated *D/MU* data within 1 to 1.5% of measured data[25,27,29,31]. In addition, studies by Fontenot *et al.*[26], Akagi *et al.*[24], and Titt *et al.*[28] indicate that absorption and scatter of the treatment beam in field-specific collimation devices, range compensators (RC), and patient anatomy have the potential to increase uncertainty in estimates of absorbed dose per monitor unit in the patient, $(D/MU)_p$, by 1% or more. In this respect, Akagi *et al.*[24] demonstrated that the combined effects of scatter in the RC, scatter in the patient, and scatter from the patient-specific collimator could yield $(D/MU)_p$ values 2% to 3% higher or lower than those measured in a phantom. These results were confounded by field-size effects, which were subsequently addressed by Titt *et al.*[28] Finally, Fontenot *et al.*[26] addressed uncertainty in *D/MU* measurements under patient-specific fields associated with the presence of the range compensator and they recommended measurement without the range compensator. Together, these works underscore the need for standard methods of determining $(D/MU)_p$ values, the potential complexities of doing so, and the need to better understand the total uncertainty in $(D/MU)_p$.

The objective of this study was to estimate total uncertainty in $(D/MU)_p$, values for patients who receive proton therapy for prostate cancer. In particular, we used treatment planning system (TPS) calculations, measurements, MC simulations, and a comparison to the historical value of 1.0 to quantify the least understood factor in the water-to-patient absorbed dose conversion factor, F_{CSPS}, the multiplicative factor that takes into account scatter from the RC and internal patient scatter, and its uncertainty.

2. Materials and Methods

2.1 *D/MU* formalism

The formalism for calculating the beam output, or *D/MU* value, for proton therapy was based in part on previously reported methods.[30,32] Our formalism includes *D/MU* estimates under reference conditions, field-specific treatment conditions, and *D/MU* estimates in the patient (Figure 1).

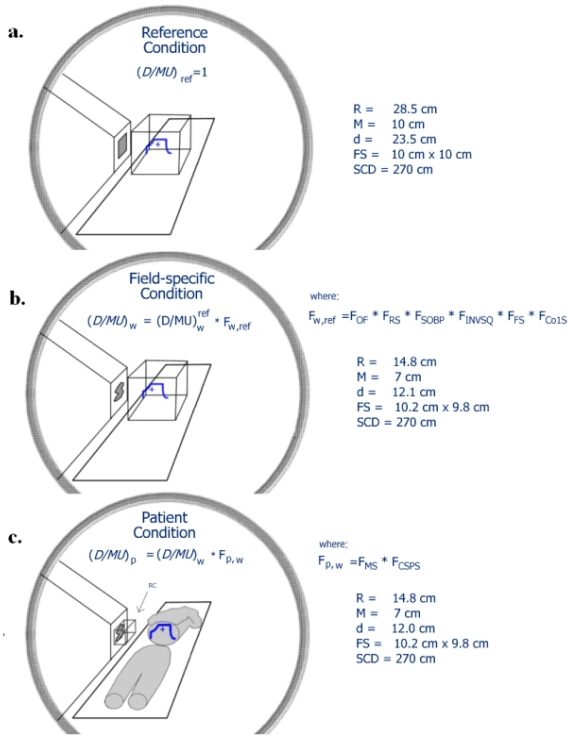

Figure 1: *Schematic diagram for the measurement formalism in the reference (a), treatment-field-specific (b), and patient (c) conditions. The parameters describing these conditions are the beam range, R; modulation, M; depth to calibration point, d; field size, FS; and source-to-calibration point distance, SCD, which is isocenter for the fields in this project. In (c) 'RC' specifies the field-specific range compensator.*

We first defined *D/MU* in a water phantom under reference conditions, shown in Figure 1a and denoted by $(D/MU)_w^{ref} \equiv 1$ cGy MU^{-1}. The reference condition comprises a collimated 10 cm × 10 cm field with a range of 28.5 cm (250 MeV proton beam), a 10-cm spread-out Bragg peak (SOBP), and a center of modulation at 23.5-cm depth in water that was located at isocenter. This range corresponds to the most penetrating beam available from the treatment unit at our institution with a medium field size. Note that a water equivalent phantom, e.g., a solid plastic phantom, may also be used. For simplicity and brevity, we shall consider these as being interchangeable.

We next defined *D/MU* value in a water phantom as before, except the proton beam parameters were taken from a treatment field (Figure 1b), as

$$\left(\frac{D}{MU}\right)_w = \left(\frac{D}{MU}\right)_w^{ref} \cdot F_{w,ref} \quad (1)$$

where $F_{w,ref}$ is a conversion factor that takes into account differences between the D/MU values at the reference condition and the treatment-field-specific condition in water. $F_{w,ref}$ is defined as

$$F_{w,ref} = \prod_i F_i = F_{OF} \cdot F_{RS} \cdot F_{SOBP} \cdot F_{InvSq} \cdot F_{FS} \cdot F_{ColS} \quad (2)$$

where F_i are as follows. F_{OF} corrects for changes in beam output which result from differences in the proton beam energy spectrum relative to the reference condition; these changes are due to differences in the properties of the beam that is injected into the treatment head and due to scatter and absorption in the range modulator wheel. F_{RS} corrects for changes in beam output due to the range shifter. F_{SOBP} corrects for changes in the beam output due to differences in the SOBP relative to the reference field. F_{InvSq} corrects for changes in beam output which result from differences in beam divergence relative to the reference condition; changes in beam divergence occur when there are changes in the distance from the effective source to the field specific point of measurement, or calibration point. (The calibration point for the reference condition was located at isocenter; the distance from the effective source to isocenter for our passively scattered beamlines was 270 cm.) F_{FS} corrects beam output for differences in proton fluence due to changes in the uncollimated field size (*i.e.*, the amount of lateral beam spreading), and F_{ColS} corrects beam output for differences in scatter from the reference aperture (10 cm x 10 cm) to the patient-specific aperture.[28]

We defined the (D/MU) value in the patient (Figure 1c) according to

$$\left(\frac{D}{MU}\right)_p = \left(\frac{D}{MU}\right)_w \cdot F_{p,w} \quad (3)$$

where, $F_{p,w}$ is a conversion factor that accounts for differences in the D/MU values between the field-specific calibration condition in water and the patient-specific treatment condition in tissue, or

$$F_{p,w} = F_{MS} \cdot F_{CSPS} \quad (4)$$

F_{MS} corrects for effect of differences in the proton mass stopping power in tissue relative to that in water. It can be determined using MC simulations or analytical calculations.[33, 34] The compensator scatter and patient scatter factor, F_{CSPS}, takes into account differences in the beam output due to differences in the scattering and attenuation within the patient and RC together relative to that of a water box phantom and no RC.

F_{CSPS} was the focus of our study and we considered two methods for estimating it. In the first method, which we shall refer to as the treatment planning system method (TPS method), we define

$$F_{CSPS} = \frac{D^p_{RC}/MU}{D^w_{no\_RC}/MU} \quad (5)$$

where D^p_{RC}/MU is the absorbed dose per MU in the patient at the calibration point (described below) with the patient-specific RC present in the field, and $D^w_{no\_RC}/MU$ is the absorbed dose per MU in water (or water equivalent material) at the calibration point without the RC in the field.

In the second method, named the treatment planning system and measurement method (TPS+M method), we approximated* F_{CSPS} as

$$F_{CSPS} \approx F_{CS} \cdot F_{PS} \quad (6)$$

where, F_{CS} corrects beam output for compensator scatter and is given by

$$F_{CS} = \frac{D^w_{RC}/MU}{D^w_{no\_RC}/MU} \quad (7)$$

and F_{PS} corrects beam output for internal patient scatter and is given by

$$F_{PS} = \frac{D^p_{RC}/MU}{D^w_{RC}/MU} \quad (8)$$

D^w_{RC}/MU in equation (7) is the absorbed dose per MU in water (or water equivalent material) at the calibration point with the RC in the field, and the other terms in equations (7) and (8) are as defined for equation (5). The calibration point is the location where the relative absorbed dose (in MU) is calibrated to the prescribed absolute absorbed dose (in Gy). It typically corresponds to a region in the patient or phantom that will receive uniform dose and is close to the center of the SOBP. Because the prostate treatment plans used in this work were isocentric, all treatment fields within a plan shared the same calibration point, *i.e.*, isocenter (IEC 1989). As such, the calibration point for each individual treatment field occupied the same point in space, whether in water or in the patient.

2.2 Uncertainty budget

We used an uncertainty budget for $(D/MU)_p$ as an *a priori* guide in studying the numerical impact of uncertainty in various factors on uncertainty in $(D/MU)_p$. Specifically, we prepared a lookup table (see Table 1) to determine which intervals of uncertainty in $(D/MU)_w$, F_{ColS}, and F_{CSPS}, respectively, would cause ≤ 5% uncertainty in $(D/MU)_p$. In it, we considered three methods for determining $(D/MU)_p$. The main difference between methods was the way in which $(D/MU)_w$ was determined, *i.e.*, through use of a TPS, measurements, or MC simulations.

* The relation is approximate because of subtle inter–relations between F_{PS} and F_{CS}, which makes it difficult to determine either one independently of the other.

Table 1: *Uncertainty budget, providing permutations of uncertainty (as a percentage) for factors in equations (9) to (11). The symbol 'μ' is used to indicate uncertainty associated with the variables in the table. Permutations are shown relative to a general outcome of 5% uncertainty for the patient-specific D/MU calculation for the cases in which $(D/MU)_w$ was estimated using TPS, measurements, and MC simulations. $\mu(D/MU)_w$ was restricted to values between 2.5% and 4.5%, and where applicable, μF_{ColS} was set to 1.0%, as was μF_{MS}.*

Method of $(D/MU)_w$ estimation	Contributing uncertainties				Combined uncertainty
	Field-specific collimator catter, μF_{ColS}	$\mu(D/MU)_w$	Compensator & patient scatter, μF_{CSPS}	Mass stopping power, μF_{MS}	$\mu(D/MU)_p$
TPS, *i.e.*, $(D/MU)_w^{TPS}$	1.0%	2.5%	3.5%	1.0%	4.5%
	1.0%	2.5%	4.0%	1.0%	4.9%
	1.0%	3.5%	3.0%	1.0%	4.8%
	1.0%	3.5%	3.5%	1.0%	5.1%
	1.0%	4.0%	2.0%	1.0%	4.7%
	1.0%	4.0%	2.5%	1.0%	4.9%
	1.0%	4.5%	1.5%	1.0%	4.9%
Measured, *i.e.*, $(D/MU)_w^{meas}$	n/a	2.5%	4.0%	1.0%	4.8%
	n/a	2.5%	4.5%	1.0%	5.2%
	n/a	3.5%	3.0%	1.0%	4.7%
	n/a	3.5%	3.5%	1.0%	5.0%
	n/a	4.0%	2.5%	1.0%	4.8%
	n/a	4.0%	3.0%	1.0%	5.1%
	n/a	4.5%	2.0%	1.0%	5.0%
Simulated with MC, *i.e.*, $(D/MU)_w^{MC}$	n/a	2.5%	4.0%	n/a	4.7%
	n/a	2.5%	4.5%	n/a	5.1%
	n/a	3.5%	3.0%	n/a	4.6%
	n/a	3.5%	3.5%	n/a	4.9%
	n/a	4.0%	2.5%	n/a	4.7%
	n/a	4.0%	3.0%	n/a	5.0%
	n/a	4.5%	2.0%	n/a	4.9%

When using a TPS to predict $(D/MU)_w$, we have

$$\left(\frac{D}{MU}\right)_p = \left(\frac{D}{MU}\right)_w^{TPS} \cdot F_{MS} \cdot F_{CSPS} \cdot F_{ColS} \quad (9)$$

where, $(D/MU)_w^{TPS}$ was estimated by the pencil beam algorithm (PBA) algorithm[35] in TPS, F_{ColS} is defined in equation (2), and F_{MS}, F_{CSPS} are defined according to equation (4). $(D/MU)_w^{TPS}$ and F_{MS} were obtained from interpolation of measured values, and F_{CSPS} was obtained using a TPS (Eclipse, Varian Medical Systems, Palo Alto, CA). However, because the TPS did not calculate the contribution of lateral scatter from the edges of the field-specific collimator[28], we included F_{ColS} (as a modifier of $(D/MU)_w$) in the estimation of $(D/MU)_p$.

When using measurements of $(D/MU)_w$ (with the patient-specific collimator in place), we have

$$\left(\frac{D}{MU}\right)_p = \left(\frac{D}{MU}\right)_w^{meas} \cdot F_{MS} \cdot F_{CSPS} \quad (10)$$

where, F_{ColS} does not appear because it is implicitly taken into account in $(D/MU)_w^{meas}$.

Finally, when $(D/MU)_w$ was estimated using MC simulations, we have

$$\left(\frac{D}{MU}\right)_p = \left(\frac{D}{MU}\right)_w^{MC} \cdot F_{CSPS} \quad (11)$$

where, $(D/MU)_w^{MC}$ inherently includes consideration of each material in the proton beam path (and its mass stopping power) as well as lateral scatter from the field-specific collimator. Thus, F_{CSPS} is the only correction factor in the equation, provided $(D/MU)_w^{MC}$ is determined in a water box phantom.

We used standard methods for error propagation to estimate the relative uncertainty in $(D/MU)_p$ as,

$$\frac{\mu\left(\frac{D}{MU}\right)_p}{\left(\frac{D}{MU}\right)_p} = \sqrt{\left(\frac{\mu\left(\frac{D}{MU}\right)_w}{\left(\frac{D}{MU}\right)_w}\right)^2 + \left(\frac{\mu(F_{ColS})}{F_{ColS}}\right)^2 + \left(\frac{\mu(F_{CSPS})}{F_{CSPS}}\right)^2 + \left(\frac{\mu(F_{MS})}{F_{MS}}\right)^2} \quad (12)$$

where, μ was the symbol used to represent uncertainty. Each quantity in equations (9) through (11) has an associated uncertainty, and several of those uncertainties were variable or unknown. Thus, the estimation of relative uncertainty in $(D/MU)_p$ (Table 1) was based on a combination of three methods, including standard propagation of errors[36], use of uncertainty values from the literature, and sensitivity testing to quantify the impact of contributing uncertainties that were not available from the literature or that were not determined in this work. The uncertainty factors $\mu(D/MU)_w$, μF_{CS}, μF_{CSPS}, and μF_{MS} were

found to be uncorrelated, and intervals of each factor were found that satisfied the 5% uncertainty criterion of $(D/MU)_p$. Values of $\mu(D/MU)_w$ were restricted to the interval from 2.5% to 4.5%, μF_{ColS} was set to 1.0%, as was μF_{MS}, and μF_{CSPS} were restricted from 1.5% to 4.5%. In other words, the results of the *a priori* estimates of relative uncertainty in $(D/MU)_p$ (Table 1) were used to estimate plausible values of the uncertainty in $(D/MU)_p$ when various values of $\mu(D/MU)_w$, μF_{ColS}, μF_{CSPS}, and μF_{MS} were taken into account.

2.3 Parameter values used to populate the uncertainty budget

Table 2 lists the parameter values used in equation (12) to populate Table 1, their associated uncertainties, and the corresponding literature sources. We used a value of 1.02 for $(D/MU)_w$ because it is typical for a prostate patient treated at our institution. However, values of $(D/MU)_w$ potentially depend on how $(D/MU)_w^{ref}$ is defined by individual facilities and the protocols they follow.[1,21,37] Therefore, an interval of $(D/MU)_w$ values was provided. This interval takes into account reported differences between the ICRU and IAEA protocols.[38,39,40] Consequently, the interval of values used to estimate the relative uncertainty in $(D/MU)_w$ was ±2.5% to ±4.5%.

The value used for F_{ColS}, 1.02, reflects the importance of the collimator in proton beam dosimetry.[28] The uncertainty for F_{ColS}, μF_{ColS}, was estimated using an interval of ±1%, which accounted for deviations in the treatment field from a 10 cm x 10 cm collimated field size, variation in beam energies from 160 MeV to 250 MeV, and variation in the location of the calibration point relative to the center of the SOBP.

The value used for F_{MS}, 1.0, is an estimate of the dosimetric effect that a medium other than water causes due to differences in the proton mass stopping powers. The uncertainty in F_{MS}, μF_{MS}, was estimated at 1% using mass stopping power ratios[41] of water to muscle.

Table 2: *Estimated parameter values and their relative uncertainties for $(D/MU)_p$. The constituent terms of equation (9) are listed with their respective values, uncertainties, and the references used to determine them. Information from* ***Table 2*** *was applied to equation (12), and those results were used to populate* ***Table 1****.*

Parameter	Estimated value(interval)	Relative uncertainty	References	Comments
$(D/MU)_w$	1.02* (0.97 – 1.007)	±2.5% - ±4.5%	IAEA[21], ICRU[37], Newhauser *et al.*[39]	IAEA[21] and ICRU[37] reported 2.0% - 2.6% uncertainty in absorbed dose measurements under reference conditions, and Newhauser *et al.*[39] reported 4.4%.
F_{ColS}	1.02 (1.01 – 1.03)	±1%	Titt *et al.*[28], Sahoo *et al.*[30], Akagi *et al.*[24]	Titt *et al.*[28] reported a 2% effect for general dosimetric accuracy and a 2.5% - 3% effect for the collimator size, energy, and SOBP used in this study, so uncertainty of ±1% was used to account for this.
F_{MS}	1.00 (1.00 – 1.02)	±1%	Siebers *et al.*[33], Paganetti[34]	Siebers *et al.*[33] reported a water-to-ICRU tissue mass stopping power factor of 1.01, which differed from water-to-cortical bone or -lung by approx. 10% or 2%, respectively.
F_{CS}	1.034 (1.034 – 1.036)	±0.20%	Akagi *et al.*[24]	Parameter values and uncertainties were measured in phantom, then manually corrected for collimator scatter.
F_{CSPS}	1.059 (1.021 – 1.097)	±3.6%	Akagi *et al.*[24]	Parameter values and uncertainties were measured in phantom, then manually corrected for collimator scatter.
	1.00	≈±4%	Sahoo *et al.*[30]	Sahoo *et al.*[30] reported 1.00±0.04 for $\overline{F_{CSPS}}$, where 1.00 is the average F_{CSPS} over 5 unspecified treatment locations and 0.04 is the standard deviation of the mean. The ratio of the mean to the standard deviation of the mean was used here to approximate relative uncertainty.
	1.03	Unknown	Akagi *et al.*[24], Sahoo *et al.*[30]	An average of F_{CSPS} values from the previous rows, *i.e.*, values estimated from data reported by Akagi *et al.*[24] and Sahoo *et al.*[30].

The values for F_{CS} and F_{CSPS} were determined using data from the only publications which directly addressed patient and compensator scatter.[24, 30] Akagi *et al.*[24] used a water phantom to determine values for F_{CS} and F_{CSPS}, and Sahoo *et al.*[30] used a commercial TPS and its verification plan feature to report a mean F_{CSPS} value of 1.00±0.04 for a sample of unspecified anatomical treatment locations. However, because neither study provided an estimate of F_{CSPS} for prostate treatment fields, we used the arithmetic average of values from Akagi *et al.*[24] and Sahoo *et al.*[30], yielding the F_{CSPS} value of 1.03 listed in Table 2. The uncertainty in our estimate of F_{CSPS} in Table 2 was unknown, thus determining a value of $\mu(F_{CSPS})$ was a central focus of this work (section 2.5) as it is needed for the estimation of uncertainty in $(D/MU)_{p.}$

2.4 Estimation of F_{CSPS} for prostate treatment fields

2.4.1 Estimation of F_{CSPS} using the TPS method

The TPS method (eq. 5) was applied to each of 32 prostate treatment fields taken from a representative sample of patients (n = 16, 2 treatment fields each) from our practice. Patients were selected using the consecutive sampling method[42] to minimize selection bias and indexed as 1 through 16. Patients in this study (1) received passively scattered proton treatments for stage I or II prostatic adenocarcinoma and (2) a *D/MU* calibration date within a year of this study's inception. The first date in the calibration interval was selected arbitrarily, and the end date was based on the date on which the desired number of consecutive patients had been treated.

To calculate absorbed dose to water (or water equivalent material), *i.e.*, $D^{w}_{no\_RC}$ in equation 5, we used the verification plan feature of the TPS, utilizing the same beam energy, lateral scatterer, range shifter, range modulation, and collimation as in the patient's treatment plan but with the patient's CT anatomy replaced by a water-box-phantom. The procedure for creating verification plans was taken from Newhauser.[43] Briefly, in all fields, the calibration point location remained fixed at isocenter (Figure 2) to minimize the dosimetric impact of differences in beam divergence. Also, as described by Newhauser[22], the water-equivalent depth of the calibration point was made equal for a treatment plan and the corresponding verification plan by shifting the water phantom in the verification plan. By maintaining the same location and water-equivalent depth of the calibration point in the patient and water phantom, dosimetric differences due to differences in scatter in the patient and phantom were isolated, so their respective effects on dose delivered to the calibration point could be revealed.

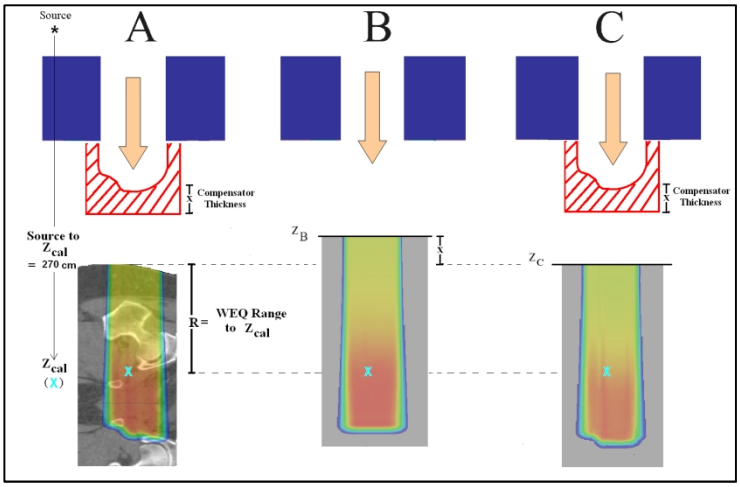

Figure 2: *Dose distributions (shown by color wash) differ between the patient and water. A right lateral prostate treatment field (A). The verification plan feature in the treatment planning system was used to apply the same treatment field to water with the range compensator not included (B) and included (C). Additionally, the position of the downstream face of the water phantom is shown relative to the patient's downstream surface in the treatment field (A) and the verification fields for the case when the range compensator is not in the beam path (B) and the case when the range compensator is in the beam path (C). When the range compensator is not present, the Z-position of the downstream face of the water phantom is given by* $Z_B = 270 - R - x$*, where x refers to the compensator thickness and R refers to the water-equivalent range to the calibration point, Zcal, (blue 'X') in the treatment field along the axis of measurement. Similarly, when the range compensator is present, the Z-position of the water phantom is given by* $Z_C = 270 - R$.

Table 3: *Summary of parameters for patients 17 and 18. Measurement point (MP) depth describes the water-equivalent depth of the calibration point from the phantom surface. This value is given both without the range compensator (no RC) in place and with it (RC). "Air gap" describes the distance between the downstream face of the treatment snout to the upstream face of the phantom. The modulator wheel identification (ID), the spread-out Bragg peak (SOBP) width, the beam energy, and penetration range were specified for each field based on the treatment plan. The penetration range and modulated width of each field are reported in water-equivalent thickness (WET). RL: right lateral; LL: left lateral.*

Patient		MP depth no RC, (RC) (cm WET)	Air gap (cm)	Modulator wheel ID	SOBP width (cm WET)	Beam energy (MeV)	Penetration range (cm WET)
17							
	RL field	19.5, (19.4)	30	155	11	250	24
	LL field	19.2, (19.1)	30	155	11	250	23.9
18							
	RL field	19.7, (19.6)	30	27	9	250	24.2
	LL field	19.5, (19.4)	30	27	9	250	23.9

2.4.2 Estimation of F_{CSPS} using the TPS+M method

The TPS-plus-measurement (TPS+M) method used a combination of measurements of absorbed dose in a water phantom and TPS calculations to estimate F_{CSPS} according to equation (6). This method was applied to four treatment fields from two patients. These patients met the same inclusion criteria as patients 1 to 16 except they were selected prospectively so that we were able to make the additional measurements required for this method. The corresponding patient indices were 17 and 18 (Table 3).

2.4.2.1 Estimation of F_{CS} using measurements

Our measurements of F_{CS}, using equation (7), utilized a 0.015-cm^3 air-filled ionization chamber (PTW pinpoint chamber, model TN31041, serial number 0079; Freiburg, Germany), an electrometer (Scandronix Wellhofer Dose 1, serial number 0293; Schwarzenbruck, Germany) and a plastic phantom (polymerized methyl methacrylate; $C_5H_3O_2$, ρ = 1.19 g cm^{-3}; GE Plastics Inc., Pittsfield, MA). Measurements were taken twice for each field: once at the calibration point with the RC in place, D^{w}_{RC}, and once at the calibration point *without* the RC in place, $D^{w}_{no\_RC}$. In the measurement for $D^{w}_{no\_RC}$, the water-equivalent thickness of the phantom was increased to preserve a fixed location of the calibration point. Finally, F_{CS} was estimated according to equation (7).

2.4.2.2. Estimation of F_{PS} using the TPS

The second step in generating F_{CSPS} values with the TPS+M method was to determine F_{PS} using equation (8). Because *in vivo* measurements were not feasible, the PBA in the TPS was used to determine the ratio of absorbed dose at the calibration point in the patient, $D^{p,cal}_{RC}$, to that in a water phantom, $D^{w,cal}_{RC}$.

2.5. Uncertainties in F_{CSPS}

2.5.1. Estimation of uncertainty in F_{CSPS} from the TPS method

When F_{CSPS} was determined using the TPS method, *i.e.*, TPS dose estimates applied to equation (5), the corresponding uncertainty in F_{CSPS}, $(\mu F_{CSPS})_{TPS}$, was estimated by comparing values of absorbed dose in the patient generated by the TPS calculations and MC simulations. As a result, we estimated that

$$(\mu F_{CSPS})_{TPS} \geq \frac{|D_{TPS} - D_{MC}|}{D_{TPS}}, \quad (13)$$

where, D_{TPS} represents absorbed dose from the TPS method at the calibration point in the patient, and D_{MC} represents absorbed dose from MC simulations at the calibration point in the patient.

In practice, we used differences in dose profiles to estimate D_{TPS} and D_{MC} for patients 17 and 18. These profiles were generated using the PBA[35] in the TPS and the Monte Carlo Proton Radiotherapy Treatment Planning (MCPRTP) code[44, 45]. In general, Contemporary proton PBAs in the TPS system provide excellent accuracy[44], especially in homogeneous media, superior to that of broad beam algorithms in heterogeneous media. The improvement in accuracy comes mostly at the cost of greater computation times. Because of inherent approximations in the PBA, it may not provide sufficient accuracy in extremely heterogeneous media, at material and/or density interfaces, or in other complex situations. The MCPRTP used the Monte Carlo N-particle eXtended radiation transport code[46] with parallel processing as a radiation dose calculation engine. Each component of the proton treatment unit was modeled in detail and patient's CT images were converted to voxelized phantom in the MCNPX code. The accuracy of the Monte Carlo simulation model has been previously evaluated by Titt *et al.*[47] More details of Monte Carlo simulations can be found in previous reports from our group.[44, 48, 49, 50]

D_{MC} was considered to provide the best estimate of the true absorbed dose at the calibration point. This

distinction was made for two reasons.(1) The MC simulation model used more complete and realistic physics models to describe multiple coulomb scattering and nuclear interactions.[27] (2) The MC simulations took into account the variations in elemental composition and mass density of various tissues, whereas the TPS approximated all tissues as water of varying density.[45] Input data to both algorithms (*i.e.*, the CT data set, aperture, RC, and beam line parameters) were identical, so differences in predicted dose distributions were attributed solely to differences in the pencil beam and Monte Carlo dose algorithms.

2.5.2. Estimation of uncertainty in F_{CSPS} from the TPS+M method

When F_{CSPS} was determined using the TPS+M method, *i.e.*, TPS dose estimates and measurements (section 2.4.2), the corresponding uncertainty in F_{CSPS}, $(\mu F_{CSPS})_{TPS+M}$, was estimated using a statistical approach: differences between F_{CSPS} values generated with the TPS+M and TPS methods were used to estimate upper and lower bounds of $(\mu F_{CSPS})_M$. The lower bound of the absolute uncertainty in F_{CSPS}, $\left[(\mu F_{CSPS})_{TPS+M}\right]_{min}$, was estimated according to

$$\left[(\mu F_{CSPS})_{TPS+M}\right]_{min} = \left|\overline{F_{CSPS(TPS)}} - \overline{F_{CSPS(TPS+M)}}\right| \quad (14)$$

where, $\overline{F_{CSPS(TPS)}}$ and $\overline{F_{CSPS(TPS+M)}}$ are the mean F_{CSPS} values from the TPS and TPS+M methods, respectively. The $\overline{F_{CSPS(TPS)}}$ value was averaged over 32 fields (patients 1-16), and the $\overline{F_{CSPS(TPS+M)}}$ value was averaged over 4 fields (patients 17 and 18). Mean values were used because it was assumed that most random variations in the data would be averaged out of the respective data sets, so the resulting difference would represent a clinically representative estimate of the differences between calculation methods, *i.e.*, a lower bound for the true uncertainty in F_{CSPS}.

The upper bound of uncertainty in F_{CSPS}, denoted by $\left[(\mu F_{CSPS})_{TPS+M}\right]_{max}$, was estimated from the maximum absolute values of difference in paired F_{CSPS} values, or

$$\left[(\mu F_{CSPS})_{TPS+M}\right]_{max} = \left|F_{CSPS(TPS)_{x_i}} - F_{CSPS(TPS+M)_{x_i}}\right|_{max} \quad (15)$$

where, the subscripts x_i indicate that the TPS and TPS+M calculations were performed for each individual field in the sample, *i.e.*, patients 17 and 18 (see section 2.4.1). Because $\left[(\mu F_{CSPS})_{TPS+M}\right]_{max}$ was calculated for each field individually, it represented the differences in the TPS and TPS+M calculation methods solely. With this approach, we avoided confounding factors such as inter-patient differences in anatomy or treatment design that would have occurred otherwise.

2.5.3. Estimation of uncertainty in F_{CSPS} from historical methods

When the historical value of 1.0 was used for F_{CSPS}, the corresponding uncertainty in F_{CSPS}, $(\mu F_{CSPS})_{HIST}$, was estimated according to,

$$(\mu F_{CSPS})_{HIST} = \left|F_{CSPS(HIST)} - F_{CSPS(TPS)}\right| \quad (16)$$

where, $F_{CSPS(HIST)}$ is 1.0 and $F_{CSPS(TPS)}$ was determined with the TPS method. This estimation was done for patients 1 through 16.

3. Results

3.1. Estimation of F_{CSPS} using the TPS method

Table 4 lists descriptive statistics that compare F_{CSPS} values from the two data sets studied here (patients 1-16 and 17-18). The $\overline{F_{CSPS}}$ values for the two data sets were not significantly different from one another.

3.2. Estimation of F_{CSPS} using the TPS+M method

Table 4 reveals good agreement between values of F_{CSPS} calculated with the TPS method and those calculated with the TPS+M method. The standard deviation in F_{CSPS} for the TPS method was smaller than the corresponding value from the TPS+M method. Also, there was a larger interval in values for the TPS+M method than for the TPS method. There are several possible explanations for this. One is that additional statistical uncertainty was introduced by the measurements. Another is that the measurements better indicate the true standard deviation, while the TPS method artificially smooths out some of the true variation.

3.3. Estimation of uncertainty in F_{CSPS}

3.3.1. Uncertainty in F_{CSPS} using the TPS method

Absorbed dose predictions from MC and pencil beam algorithms were compared for a prostate treatment in one of the patients (patient 17) following the methods of 2.5.1. Differences in estimates of absorbed dose between MC simulations and the TPS method resulted in a 10.5 cGy difference between profiles at isocenter for the right lateral field and a 4.7 cGy difference for the left lateral field. The absorbed doses from the right and left lateral fields for the treatment plan at isocenter, which were used to represent D_w as an approximation, were 3550 cGy and 3570 cGy, respectively. Therefore, the $(\mu F_{CSPS})_{TPS}$ was less than 0.3% for the individual fields. These estimates suggest that the contribution of μF_{CSPS} to uncertainty in $(D/MU)_p$ for this particular patient was negligible.

Table 4: *Statistics for F_{CSPS} using the TPS and TPS+M (TPS plus measurement) methods. The mean F_{CSPS}, standard deviation, and minimum and maximum F_{CSPS} values are listed for three data sets. In the two center columns, F_{CSPS} values were calculated with equation (5) using the TPS method. In the last column, F_{CSPS} values were calculated with equation (6), using measurements for F_{CS} and pencil beam predictions for F_{PS} using the TPS+M method. The fields used to generate data in the two rightmost columns differed from those used in the second column.*

Parameter	Calculation Method		
	TPS*	TPS**	TPS+M**
Number of patients	16	2	2
Number of fields	32	4	4
Mean F_{CSPS}	1.006	1.004	1.002
Standard deviation	0.008	0.008	0.013
Standard deviation of the mean	0.001	0.004	0.007
Minimum F_{CSPS}	0.990	0.992	0.988
Maximum F_{CSPS}	1.029	1.012	1.018

Table 5: *Statistics for μF_{CSPS} using differences between the TPS method, the TPS+M (TPS + measurements) method, MC (Monte Carlo) simulations, and the historical value of 1.0. Estimates of μF_{CSPS} were determined from differences between calculation methods for absorbed dose at isocenter in typical prostate treatment fields.*

Parameter	Comparison		
	TPS** vs. TPS+M**	TPS** vs. MC**	TPS* vs. 1.0*
Number of patients	2	1 (patient 17)	16
Number of fields	4	2	32
Mean μF_{CSPS}	0.006	0.002	0.006
Standard deviation	n/a	n/a	0.008
Standard deviation of the mean	n/a	n/a	0.001
Minimum μF_{CSPS}	0.004	0.001	0.010
Maximum μF_{CSPS}	0.008	0.003	0.029

3.3.2. Uncertainty in F_{CSPS} using the TPS+M method

Following the methods in section 2.5.2, we estimated the upper and lower bounds for uncertainty in F_{CSPS}. The lower bound, $\left[(\mu F_{CSPS})_{TPS+M}\right]_{min}$, was 0.004 and the upper bound, $\left[(\mu F_{CSPS})_{TPS+M}\right]_{max}$, was 0.008.

3.3.3. Uncertainty in F_{CSPS} using the historical estimate

Estimates of F_{CSPS} done using the TPS method were compared to the historical value of 1.0 for F_{CSPS}. Descriptive statistics for this analysis are listed in Table 5. The $(\mu F_{CSPS})_{HIST}$ was less than 0.029, and the mean $(\mu F_{CSPS})_{HIST}$ was 0.006.

4. Discussion

We estimated uncertainty in $(D/MU)_P$ for patients receiving proton therapy for cancer of the prostate. In particular, we compared estimates of uncertainty in F_{CSPS} by means of measurements, MC simulations, and pencil beam dose calculations. Our results confirm that when F_{CSPS} is included in the estimation of $(D/MU)_P$, the uncertainty in $(D/MU)_P$ is less than 5%, regardless of the method used to calculate F_{CSPS}.

Our findings on F_{CSPS} are similar to those of Newhauser[22,51] and Sahoo *et al.*[30] At the outset of this work, the standard of care at our institution followed the approach described by Newhauser[22] in which F_{CSPS} was taken as unity. Subsequently Newhauser *et al.*[51] reported that F_{CSPS} for prostate treatment fields was near the historical value of 1.0 based on results of a phantom study. Likewise, Sahoo *et al.*[30] reported that F_{CSPS} spanned the interval 0.957 to 1.089 with a mean value of 1.00 ± 0.04. However, we note that Sahoo *et al.*[30] did not specify which anatomical treatment sites these values were from. Therefore, it is difficult to make a direct comparison of those results with the findings from this work.

As noted in section 2.3, we found no directly comparable reports on μF_{CSPS} in the literature for prostate treatment. Our findings on μF_{CSPS} differ from those in the works most similar to ours, that is, reports from Akagi *et al.*[24] and Sahoo *et al.*[30]. Akagi *et al.*[24] reported a relative uncertainty of 3.6% in the measured value of F_{CSPS}; this value exceeds ours by approximately a factor of 10. However, the uncertainty reported by Akagi *et al.*[24] took into account the errors in reproducing collimator scatter (F_{ColS}) and inaccuracy in analytical modeling of patient anatomy which were not applicable to our study.

One of the clinical implications of this work is that accuracy of $(D/MU)_P$ values, in the special case of prostate treatment fields, does not depend strongly on accurate knowledge of the F_{CSPS} factor. Thus, this work also provides

an evidential basis and rationale for standardizing absolute proton dosimetry, which is a key requisite step to conduct multi-institution clinical trials.

This study had several limitations. First, it considered normal patient anatomy, *e.g.*, the effects of implanted fiducial markers, hip prostheses, and organ motion on $(D/MU)_p$ and its uncertainty were not included. However, these are not serious limitations because solutions for fiducial markers are known[52,53,54,55], and although hip prostheses are relatively rare, there are MV/kV imaging solutions that are available to correct for their effects[56]. Second, we considered only the lateral opposed-pair treatment technique, while involvement of pelvic lymph nodes or treatment of other more complex treatment strategies[57,58] would require a much different application of our present findings. Third, our findings are specific to the treatment planning and delivery systems in use at our institution for a passively scattered treatment; there may be additional differences between this study and other treatment techniques, such as intensity-modulated proton therapy. Nonetheless, the methods and results of this study may serve as a qualitative guide for similar studies of other proton therapy systems.

Given the complexities and uncertainties associated with estimation of absorbed dose in the patient, additional studies are needed to test whether the findings of this work will hold for other anatomical sites. In our laboratory, additional studies are now under way to address estimation of uncertainties in $(D/MU)_p$ in the thorax.

5. Conclusion

In conclusion, our study investigated the water-to-patient absorbed dose conversion factor, F_{CSPS}, one of the least well-understood factors in proton output calculation, and found that mean F_{CSPS} value was 1.006 and uncertainty in F_{CSPS} was approximately 1%, suggesting that uncertainty in F_{CSPS} for proton therapy of prostate cancer is clinically acceptable.

Conflict of Interest

The authors declare that they have no conflicts of interest. The authors alone are responsible for the content and writing of the paper.

References

1. International Commission on Radiation Units and Measurements (ICRU) 2007 Prescribing, Recording, and Reporting Proton-Beam Therapy. ICRU Report 78 (Bethesda, MD: ICRU).
2. Durante M, Loeffler JS. Charged particles in radiation oncology. Nat Rev Clin Oncol. 2010; 7:37-43.
3. PTCOG, 2014 PTCOG patient statistics of particle therapy centers in 2013.
4. Sisterson J. Ion beam therapy in 2004. Nucl Instr Meth B. 2005;241: 713-6.
5. Siegel R, Naishadham D, Jemal A. Cancer statistics, 2012. CA: Cancer J Clin. 2012;62:10-29.
6. Slater JD, Rossi CJ Jr, Yonemoto LT, *et al*. Proton therapy for prostate cancer: the initial Loma Linda University experience. Int J Radiat Oncol Biol Phys. 2004;59:348-52.
7. Rossi CJ Jr. Conformal proton beam radiation therapy for prostate cancer: concepts and clinical results. Commun Oncol. 2007;4:235-50.
8. Mayahara H, Murakami M, Kagawa K, *et al*. Acute morbidity of proton therapy for prostate cancer: the Hyogo Ion Beam Medical Center experience. Int J Radiat Oncol Biol Phys 2007;69:434-43.
9. Vargas C, Mahajan C, Fryer A, *et al*. Rectal dose-volume differences using proton radiotherapy and a rectal balloon or water alone for the treatment of prostate cancer. Int J Radiat Oncol Biol Phys. 2007;69:1110-6.
10. Coen JJ, Zietman AL. Proton radiation for localized prostate cancer. Nat Rev Urol. 2009;6: 324-30.
11. Chera BS, Vargas C, Morris CG, *et al*. Dosimetric study of pelvic proton radiotherapy for high-risk prostate cancer. Int J Radiat Oncol Biol Phys. 2009;75:994-1002.
12. Mendenhall NP, Li Z, Hoppe BS, *et al*. Early outcomes from three prospective trials of image-guided proton therapy for prostate cancer. Int J Radiat Oncol Biol Phys. 2012;82:213-21.
13. Sheets NC, Goldin GH, Meyer AM, *et al*. Intensity-modulated radiation therapy, proton therapy, or conformal radiation therapy and morbidity and disease control in localized prostate cancer. JAMA. 2012;307:1611-20.
14. Zietman AL, DeSilvio ML, Slater JD, *et al*. Comparison of conventional-dose vs high-dose conformal radiation therapy in clinically localized adenocarcinoma of the prostate: a randomized controlled trial. JAMA. 2005;294:1233-9.
15. Zietman AL, Bae K, Slater JD, *et al*. Randomized trial comparing conventional-dose with high-dose conformal radiation therapy in early-stage adenocarcinoma of the prostate: long-term results from proton radiation oncology group/american college of radiology 95-09. J Clin Oncol 2010;28:1106-11.
16. Olsen DR, Bruland OS, Frykholm G, Norderhaug IN. Proton therapy - a systematic review of clinical effectiveness. Radiother Oncol. 2007; 83:123-32.
17. Terasawa T, Dvorak T, Ip S, *et al*. Systematic review: charged-particle radiation therapy for cancer. Ann Intern Med. 2009;151:556-65.
18. AAPM. Report 16 – Protocol for heavy charged-particle therapy beam dosimetry. New York, NY:

AIP - American Association of Physicists in Medicine, Task Group 20, 1986.
19. Vynckier S, Bonnett DE, Jones DTL. Code of practice for clinical proton dosimetry. Radiother Oncol. 1991;20:53-63.
20. Vynckier S, Bonnett D E, Jones DTL. Supplement to the code of practice for clinical proton dosimetry. Radiother Oncol. 1994;32:174-79.
21. International Atomic Energy Agency (IAEA). Absorbed dose determination in external beam radiotherapy. IAEA Technical Report Series 398, 2000 (Vienna: IAEA).
22. Newhauser W. Dosimetry for the gantry beams at the Northeast Proton Therapy Center Part I: Dimensions and geometric relationships. Massachusetts General Hospital, Report HD-112, 2001.
23. Kooy HM, Rosenthal SJ, Engelsman M, *et al*. The prediction of output factors for spread-out proton Bragg peak fields in clinical practice. Phys Med Biol. 2005;50:5847-56.
24. Akagi T, Kanematsu N, Takatani Y, *et al*. Scatter factors in proton therapy with a broad beam. Phys Med Biol. 2006;51:1919-28.
25. Paganetti H. Monte Carlo calculations for absolute dosimetry to determine machine outputs for proton therapy fields. Phys Med Biol. 2006;51:2801-12.
26. Fontenot JD, Newhauser WD, Bloch C, *et al*. Determination of output factors for small proton therapy fields. Med Phys. 2007;34:489-98.
27. Herault J, Iborra N, Serrano B, Chauvel P. Spread-out Bragg peak and monitor units calculation with the Monte Carlo code MCNPX. Med Phys. 2007; 34:680-8.
28. Titt U, Zheng Y, Vassiliev ON, Newhauser WD. Monte Carlo investigation of collimator scatter of proton-therapy beams produced using the passive scattering method. Phys Med Biol. 2008; 53:487-504.
29. Koch N, Newhauser WD, Titt U, *et al*. Monte Carlo calculations and measurements of absorbed dose per monitor unit for the treatment of uveal melanoma with proton therapy. Phys Med Biol. 2008;53:1581-94.
30. Sahoo N, Zhu X, Arjomandy B, *et al*. A procedure for calculation of monitor units for passively scattered proton radiotherapy beams. Med Phys. 2008;35:5088-97.
31. Koch N , Newhauser WD. Development and verification of an analytical algorithm to predict absorbed dose distributions in ocular proton therapy using Monte Carlo simulations. Phys Med Biol. 2010;55:833-53.
32. Moyers MF, Vatnitsky SM. Practical implementation of light ion beam treatments. Medical Physics Publishing, Madison, WI, 2012. ISBN 978-1-930524-55-2.
33. Siebers JV, Keall PJ, Nahum AE, Mohan R. Converting absorbed dose to medium to absorbed dose to water for Monte Carlo based photon beam dose calculations. Phys Med Biol. 2000;45:983-95.
34. Paganetti H. Dose to water versus dose to medium in proton beam therapy. Phys Med Biol. 2009;54:4399-421.
35. Schaffner B, Pedroni E, Lomax A. Dose calculation models for proton treatment planning using a dynamic beam delivery system: an attempt to include density heterogeneity effects in the analytical dose calculation. Phys Med Biol. 1999; 44:27-41.
36. Mohr PJ, Taylor BN. CODATA recommended values of the fundamental physical constants: 1998. Rev Mod Phys 2000;72:351-495.
37. International Commission on Radiation Units and Measurements (ICRU). Clinical Proton Dosimetry Part I: Beam production, beam delivery and measurement of absorbed dose. ICRU Report 59, 1998 (Bethesda, MD: ICRU).
38. Medin J, Andreo P, Vynckier S. Comparison of dosimetry recommendations for clinical proton beams. Phys Med Biol. 2000;45:3195-211.
39. Newhauser W, Myers K, Rosenthal S, Smith AR. Proton beam dosimetry for radiosurgery: implementation of the ICRU Report 59 at the Harvard Cyclotron Laboratory. Phys Med Biol. 2002;47:1369-89.
40. Newhauser WD, Burns J, Smith AR. Dosimetry for ocular proton beam therapy at the Harvard Cyclotron Laboratory based on the ICRU Report 59. Med Phys. 2002;29:1953-61.
41. International Commission on Radiation Units and Measurements (ICRU). Stopping powers and ranges for proton and alpha particles. ICRU Report 49, 1993 (Bethesda, MD: ICRU).
42. Lunsford TK, Lunsford BR. The research sample, Part I: Sampling. J Prosthet Orthot 1995;7:105-12.
43. Newhauser W. Procedure for creating a verification plan in the Eclipse treatment planning system for patients receiving proton therapy for cancer of the prostate, Report MDACC-10-0043, University of Texas MD Anderson Cancer Center, Houston, TX, 2007.
44. Newhauser W, Fontenot J, Zheng Y, *et al*. Monte Carlo simulations for configuring and testing an analytical proton dose-calculation algorithm. Phys Med Biol. 2007;52:4569-84.
45. Newhauser W, Zheng Y, Taddei P, *et al*. Monte Carlo proton radiation therapy planning calculations Trans. Am Nucl Soc. 2008;99:63.
46. Hendricks J, McKinney G, Durkee J, *et al*. MCNPX, Version 26c (Los Alamos, NM: Los Alamos National Laboratory) 2006.

47. Titt U, Sahoo N, Ding X, et al. Assessment of the accuracy of an MCNPX-based Monte Carlo simulation model for predicting three-dimensional absorbed dose distributions. Phys Med Biol. 2008;53:4455-70.
48. Taddei PJ, Mirkovic D, Fontenot JD, *et al*. Stray radiation dose and second cancer risk for a pediatric patient receiving craniospinal irradiation with proton beams. Phys Med Biol 2009;54:2259-75.
49. Zhang R, Fontenot J, Mirkovic D, *et al*. Advantages of MCNPX-based lattice tally over mesh tally in high-speed Monte Carlo dose reconstruction for proton radiotherapy. Nucl Technol. 2013; 183:101-6.
50. Newhauser W, Zhang R. The physics of proton therapy. Phys. Med. Biol. 2015;60:R155-209.
51. Newhauser W, Zhu R, Sahoo N, *et al*. Small corrections to measured D/MU values for patients receiving proton therapy for cancer of the prostate, Report MDACC-10-0065, University of Texas MD Anderson Cancer Center, Houston, TX, 2007.
52. Newhauser W, Fontenot J, Koch N, *et al*. Monte Carlo simulations of the dosimetric impact of radiopaque fiducial markers for proton radiotherapy of the prostate. Phys Med Biol. 2007;52:2937-52.
53. Giebeler A, Fontenot J, Balter P, *et al*. Dose perturbations from implanted helical gold markers in proton therapy of prostate cancer. J Appl Clin Med Phys. 2009;10:2875.
54. Cheung J, Kudchadker RJ, Zhu XR, *et al*. Dose perturbation and image artifacts caused by carbon-coated ceramic and stainless steel fiducials used in proton therapy for prostate cancer. Phys Med Biol. 2010;55:7135-47.
55. Huang JY, Newhauser WD, Zhu XR, *et al*. Investigation of dose perturbations and the radiographic visibility of potential fiducials for proton radiation therapy of the prostate. Phys Med Biol. 2011;56:5287-302.
56. Newhauser WD, Giebeler A, Langen KM, *et al*. Can megavoltage computed tomography reduce proton range uncertainties in treatment plans for patients with large metal implants? Phys Med Biol. 2008;53:2327-44.
57. Rechner LA, Howell RM, Zhang R, *et al*. Risk of radiogenic second cancers following volumetric modulated arc therapy and proton arc therapy for prostate cancer. Phys Med Biol. 2012;57:7117-32.
58. Rechner LA, Howell RM, Zhang R, Newhauser WD. Impact of margin size on the predicted risk of radiogenic second cancers following proton arc therapy and volumetric modulated arc therapy for prostate cancer. Phys Med Biol. 2012;57:N469-79.